The 1997 Fluids Engineering Division Summer Meeting
FEDSM'97
June 22-26, 1997

FEDSM97-3371

A PARAMETRIC EVALUATION OF THE EFFECT OF INLET SWIRL ON THE ROTORDYNAMIC FORCES GENERATED BY DISCHARGE-TO-SUCTION LEAKAGE FLOWS IN SHROUDED CENTRIFUGAL PUMPS

ROBERT V. UY, BRIAN L. BIRCUMSHAW, AND CHRISTOPHER E. BRENNEN
DIVISION OF ENGINEERING AND APPLIED SCIENCE
CALIFORNIA INSTITUTE OF TECHNOLOGY
PASADENA, CALIFORNIA 91125
TEL:(818)395-4153, FAX: (818)568-2719, BOBUY@CCO.CALTECH.EDU

ABSTRACT

Unsteady forces generated by the fluid flow through the impeller leakage path of a centrifugal pump were investigated. The effect of leakage path inlet (pump discharge) swirl on the rotordynamic forces was examined for various ratios of fluid tangential velocity to impeller tip speed. It was observed that changing the inlet swirl velocity does not appear to significantly affect the measured forces for a given leakage flow coefficient. A bulk flow numerical model was found to predict the same general result. The model agreed with experimental data for small values of the leakage flow coefficient.

NOMENCLATURE

$[A^*]$	Rotordynamic force matrix
B	Depth of logarithmic spiral channel on swirl vane
C	Direct damping coefficient, normalized by $\rho\pi\omega^2 R_2^2 L\varepsilon$
c	Cross-coupled damping coefficient, normalized by $\rho\pi\omega^2 R_2^2 L\varepsilon$
$F_x^*(t)$	Lateral horizontal force in the laboratory frame
$F_y^*(t)$	Lateral vertical force in the laboratory frame
F_{ox}^*	Time-averaged horizontal force
F_{oy}^*	Time-averaged vertical force
F_n^*	Force normal to whirl orbit
F_n	Force normal to whirl orbit normalized by $\rho\pi\omega^2 R_2^2 L\varepsilon$
F_t^*	Force tangent to whirl orbit
F_t	Force tangent to whirl orbit normalized by $\rho\pi\omega^2 R_2^2 L\varepsilon$
F_1,F_2	Lateral forces in the rotating frame
H	Clearance between impeller shroud and housing
h	Film thickness
K	Direct stiffness coefficient, normalized by $\rho\pi\omega^2 R_2^2 L\varepsilon$
k	Cross-coupled stiffness coefficient, normalized by $\rho\pi\omega^2 R_2^2 L\varepsilon$
L	Axial length of the impeller
M	Direct added mass coefficient, normalized by $\rho\pi\omega^2 R_2^2 L\varepsilon$
mr, ms	Empirical exponent for rotor and stator respectively
nr, ns	Empirical constants for rotor and stator respectively
Q	Volumetric leakage flow rate
R_2	Radius of impeller and leakage inlet
u_s	Mean leakage inlet path velocity of fluid
u_θ	Mean leakage inlet swirl velocity of fluid
x^*(t)	Horizontal displacement of impeller on its orbit

y^*(t)	Vertical displacement of impeller on its orbit
α	Turning angle of logarithmic spiral channel on swirl vane
,	Leakage inlet swirl ratio, $u_\theta/\omega R_2$
η	Dynamic viscosity
ε	Eccentricity of whirl orbit
ρ	Fluid density
ϕ	Leakage flow coefficient, $u_s/\omega R_2$
ω	Main shaft radian frequency
Ω	Whirl radian frequency
τ	Wall shear stress

INTRODUCTION

Previous experimental and analytical results have shown that discharge to suction leakage flows in the annulus of a shrouded centrifugal pump contribute substantially to the fluid induced rotordynamic forces (Adkins and Brennen 1988). Experiments conducted in the Rotor Force Test Facility (RFTF) at Caltech on an impeller undergoing a predetermined whirl have shown that the leakage flow contributions to the normal and tangential forces can be as much as 70% and 30% of the total, respectively (Jery 1986). Other experiments have examined the consequences of leakage flows and have shown that the rotordynamic forces are functions not only of whirl ratio, but also of the leakage flow rate and the impeller shroud to pump housing clearance. The forces were found to be inversely proportional to the clearance. A region of forward subsynchronous whirl was found for which the average tangential force was destabilizing. This region decreased with increasing flow coefficient (Guinzburg et al. 1994).

Guinzburg et al. (1993) previously examined the difference in rotordynamic forces with and without a prescribed inlet swirl. The tangential force increased in the presence of inlet swirl, and hence the effect of inlet swirl was found to be destabilizing. Later studies by Sivo et al. (1995) examined the effectiveness of anti-swirl brakes in reducing the destabilizing region of forward whirl.

The present paper describes a parametric evaluation of the effect of leakage path inlet swirl on the measured rotordynamic forces. The experiments use a contoured shroud and casing which are more typical of leakage path geometries than the conical shroud and casing used previously by Guinzburg et al. (1992, 1993, 1994) and Sivo et al. (1994, 1995).

ROTORDYNAMIC FORCES

Figure 1 shows a schematic of the hydrodynamic forces that act on a rotating impeller whirling in a circular orbit. F_x^* and F_y^* are the instantaneous lateral forces in the laboratory frame, Ω is the whirl radian frequency, and ω is the main shaft radian frequency. The eccentricity of the orbit is given by ε. The lateral forces are given in linear form as:

$$\begin{pmatrix} F_x^*(t) \\ F_y^*(t) \end{pmatrix} = \begin{pmatrix} F_{ox}^* \\ F_{oy}^* \end{pmatrix} + [A^*] \begin{pmatrix} x^*(t) \\ y^*(t) \end{pmatrix} \quad (1)$$

where F_{ox}^* and F_{oy}^* are the steady forces which result from flow asymmetries in the volute and $[A^*]$ is the rotordynamic force matrix. It is a function of the mean flow conditions, pump geometry, whirl frequency ratio, Ω/ω, and, if outside the linear range, may also be a function of the eccentricity, ε. In the case of a circular whirl orbit:

$$x^*(t) = \varepsilon \cos(\Omega t) \quad (2)$$

$$y^*(t) = \varepsilon \sin(\Omega t) \quad (3)$$

The normal and tangential forces for a circular whirl orbit are given by (Jery 1986):

$$F_n^*(t) = \frac{1}{2}(A_{xx}^* + A_{yy}^*)\varepsilon \quad (4)$$

$$F_t^*(t) = \frac{1}{2}(-A_{xy}^* + A_{yx}^*)\varepsilon \quad (5)$$

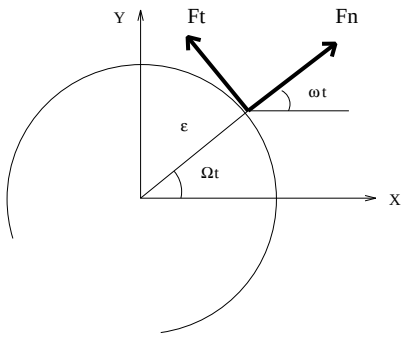

FIGURE 1: Schematic of the Fluid Induced Forces Acting on an Impeller Whirling in a Circular Orbit

ROTORDYNAMIC COEFFICIENTS AND STABILITY

To study the stability of an impeller, it is convenient for rotordynamicists to fit the dimensionless normal force, F_n, to a quadratic function of the whirl frequency ratio, Ω/ω, and to fit the dimensionless tangential force, F_t, to a linear function. The resulting expressions are given by:

$$F_n = M\left(\frac{\Omega}{\omega}\right)^2 - c\left(\frac{\Omega}{\omega}\right) - K \quad (6)$$

$$F_t = -C\left(\frac{\Omega}{\omega}\right) + k \quad (7)$$

where the dimensionless coefficients are the direct added mass (M), direct damping (C), cross-coupled damping (c), direct stiffness (K), and the cross-coupled stiffness (k). As can be seen from equation (7), a positive cross-coupled stiffness is destabilizing because it promotes whirl motion of the impeller for a range of positive sub-synchronous frequencies. The cross-coupled stiffness is also the tangential force acting at zero whirl ratio. Equation (6) indicates that a large negative direct stiffness is also destabilizing since it promotes a positive normal force which would tend to increase the eccentricity of the whirl orbit.

A convenient measure of the rotordynamic stability is the ratio of cross-coupled stiffness to the direct damping (i.e. k/C) which is termed the whirl ratio. This defines the range of positive whirl frequency ratios for which the tangential force is destablizing.

TEST APPARATUS

The present experiments were conducted in the Rotor Force Test Facility (RFTF) at Caltech (Jery 1986). The leakage flow test section of the facility is schematically shown in Figure 2. The test section isolates the leakage flow forces by using a solid impeller. The working fluid is water. The main components of the test section apparatus consist of a solid or dummy impeller (the rotating shroud), a housing (the stationary shroud), the rotating dynamometer (or internal force balance), an eccentric whirl mechanism, a leakage exit seal ring and a leakage inlet swirl vane.

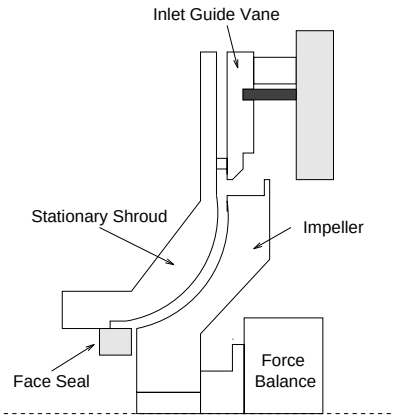

FIGURE 2: Experimental Setup

The geometry of the leakage path was modified from the conical rotor and stator used in past experiments (Guinzburg et al. 1992, 1993, 1994, Sivo et al. 1994, 1995). A rotor was designed with a third order curve fit such that the contour was parallel to the centerline at the eye and perpendicular to the centerline at the tip. A matching stator was constructed to maintain a constant normal clearance $H = 0.305$ cm. This geometry was designed to more closely model a typical centrifugal pump impeller shroud.

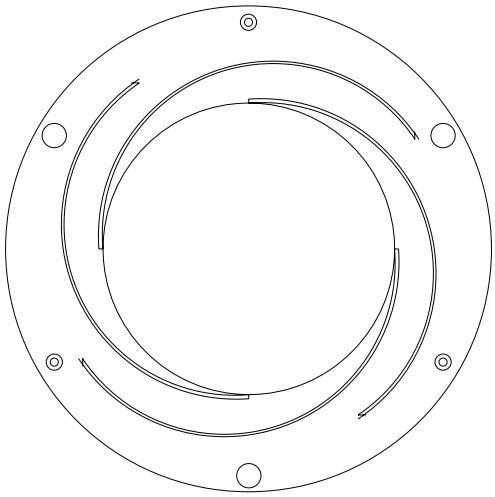

FIGURE 3: Inlet guide vane, 6 degree turning angle

The rotor is mounted directly to the rotating dynamometer connected to a data acquisition system which permits measurements of the rotordynamic force matrix components (Jery 1986). The eccentric drive mechanism imposes a circular whirl orbit on the basic main shaft rotation. The radius of the whirl orbit (eccentricity) can be varied but this set of experiments used one eccentricity $\varepsilon = 0.025$ cm. The seal ring at the leakage exit models a wear ring. The clearance between the face seal and the impeller face is adjustable. Flow through the leakage path is generated by an auxiliary pump.

The effect of inlet swirl was investigated by installing a swirl vane at the leakage inlet to introduce pre-rotation in the direction of shaft rotation. Figure 3 shows a typical vane consisting of a logarithmic spiral channel with a turning angle of 6 degrees. The swirl ratio, , (the ratio of the leakage flow circumferential velocity to the impeller tip velocity) is varied by changing the leakage flow rate and the turning angle. The swirl ratio depends on the flow coefficient and turning angle according to:

$$\frac{,}{\phi} = \frac{H}{B \tan \alpha} \tag{8}$$

where $B = 0.318$ cm. is the depth of the logarithmic spiral channel. A derivation of equation (8) (which assumes all leakage flow is constrained along the vane) is found in Guinzburg et al. (1993). For the present tests, three vanes with turning angles of $1^o, 2^o$, and 6^o were constructed to allow variation of α or ϕ while maintaining the same , .

BULK FLOW MODEL

A bulk flow model of the discharge-to-inlet leakage flow was developed by Childs (1989)(and used by Guinzburg (1992)). This model was employed, (with some modifications) in the present paper to compare with the experimental results.

The bulk flow model predicted large resonances in the calculated forces for cases in which inlet swirl was present. It was observed that these resonances could be substantially reduced if, in Childs' (1989) analysis, the β_0 and β_1 factors of the path velocity term $A_{3\theta}$ in the first-order circumferential momentum equation were set to zero.

The frictional coefficients used by Guinzburg (1992) in her calculations using Childs' (1989) theory were based on the work of Yamada (1962) and are defined by:

$$\frac{\tau}{\frac{1}{2}\rho u^2} = n\left(\frac{\rho u h}{\eta}\right)^m \tag{9}$$

where u is a mean flow velocity in the annulus and the m and n are denoted by ms and ns for the stator and mr and nr for the rotor. These are based originally on the work of Hirs (1973) who does, however, recommend that the coefficients m and n be "fitted to individual experiments." The frictional coefficients are dependent on six physical parameters, including the curvature of the surface, inertial effects, and roughness. Thus, the coefficients may not fully account for the curvature of the present rotor or the inertial effects due to the curved path of the bulk flow. Nor will the roughness parameters neccessarily agree. Given the ease with which the frictional factors can be altered in the computational model, an attempt was made to fit the model to the pre-existing experimental results. The frictional coefficients ns and nr were changed independently and the results were then compared with the experimental data. The values ms = -0.25 and mr = -0.25 were retained as they correspond to the fully turbulent flow which occurs in the annulus.

One of the approximations of Childs bulk flow model is the assumption of a single gap-averaged bulk velocity to describe the flow at any location in the annulus. Thus the model will encounter serious error when there exists regions of more complex velocity profiles with, for example, flow reversals which could even cause the shear stress to be of the opposite sign to that anticipated by equation (9) where the shear stress is correlated with the single bulk velocity. To examine the potential for such errors, Sivo et al. (1994) used a laser doppler velocimeter (LDV) to measure the velocity profile of the leakage flow. Flow reversal close to rotor shroud was observed, in agreement with computations performed by Baskharone and Hensel (1993). The recirculation occurs at different locations in the leakage path for different conditions, and seems to diminish at higher whirl ratios. In some cases, the recirculation regions are observed around the entire impeller. This reversal in flow direction near the impeller implies a serious error in the correlation of equation (9). The sign of the wall-shear stress term for the rotor should change in a region of reverse flow. This could, in part, be incorporated into the bulk flow analysis by using smaller values of nr.

RPM	Ω/ω	,	Q(gpm)	ϕ
1000	-.7 to .7	0.4	4.08	0.014
			12.21	0.043
		0.5	2.54	0.009
			5.07	0.018
			15.26	0.055
		0.6	3.05	0.011
			6.10	0.022
			18.32	0.066
		0.7	3.54	0.013
			7.08	0.025

TABLE 1: Test matrix of flow parameters

RPM	Ω/ω	,	ns	nr
1000	-1 to 1	0.6	0.13	0.08
			0.08	0.13
			0.08	0.01

TABLE 2: Test matrix of bulk-flow parameters

TEST MATRIX

The tests listed in Table 1 were conducted to measure the rotordynamic forces in the simulated leakage flow while varying parameters such as , and ϕ. For all tests a nominal clearance of H = 0.305 cm, a whirl eccentricity of ε = 0.025 cm and a leakage exit face seal clearance of 0.051 cm were used. The ranges of , and ϕ were selected to match typical pump operating conditions, as well as account for the limitations of the RFTF.

The tests listed in Table 2 were conducted to calculate the rotordynamic forces in the bulk-flow model while varying the frictional parameters ns and nr. The exponents ms =-0.25 and mr = -0.25 were held constant. Computations were performed over the same range of flow coefficients as the experimental tests, and data from the experiments such as the inlet and discharge pressures were used as inputs to the computer program.

EXPERIMENTAL RESULTS

Figure 4 shows plots of the dimensionless rotordynamic force coefficients obtained from the experiments as functions of the leakage flow coefficient. The cross-coupled stiffness appears to remain at an almost constant level for various values of , , while the direct damping shows a tendency to first increase and then decrease slightly with increasing flow coefficient. This leads to a whirl ratio, k/C in Figure 5, that increases with increasing flow coefficient. This is counter to what was observed by both Guinzburg et al. (1994) and Sivo et al. (1995). This tangential force therefore does not exhibit a substantial reduction as the flow coefficient increases. As this trend has been observed with all tests of the new contoured impeller, it appears that there are differences in the behaviour of the tangential force depending on the geometry of the leakage path.

Upon examination of the coefficients which determine the normal force, the same trends for M, c, and K observed for the conical impeller by Sivo et al. (1995) are also noted in the present experiments. The magnitudes of each normal force coefficient are also similar. In summary, it appears as though the inlet swirl has little effect on the experimental rotordynamic coefficients.

BULK FLOW ANALYSIS RESULTS

The rotordynamic force coefficients obtained from the bulk flow model are presented in Figure 6. All results presented are for a swirl ratio, , $= 0.6$. The coefficients are virtually independent of , within the range of expected values of this parameter. Using the frictional coefficients given in the figure, the results show some qualitative agreement with the experimental data. The variation in ns and nr appears to have some effect on the calculated forces. The cross-coupled stiffness appears to dramatically increase, while the direct damping appears to be slightly underpredicted and increasing gradually with increasing flow coefficient. This leads to a whirl ratio in Figure 7 which increases, as observed experimentally, but is overpredicted in magnitude.

The coefficients for the normal force appear to duplicate the general trends observed in the experiments more closely than those for the tangential force. The slight increase in the direct added mass term with flow coefficient is observed in the calculations, but the absolute magnitude is underpredicted slightly. The cross-coupled damping term matches the increase with flow, but appears to overpredict the magnitude at higher flow coefficients. The direct stiffness term shows the same tendency to decrease with increasing flow.

It appears as though the choice of frictional coefficients given in the figure can model the direct and cross-coupled stiffness, the cross-coupled damping, and the direct added mass at low flow coefficients ($0 < \phi < 0.03$). However, at higher flow coefficients ($\phi > 0.05$) the model appears to depart from an accurate prediction of any of the coefficients. The underprediction of the direct damping leads to an overestimate of the whirl ratio and hence of the unstable region of forward whirl. The limitations in the bulk flow model could be due to its assumption of a simple velocity profile and the implied shear stresses which result from that assumption. It is postulated that the flow profile may change significantly as the flow rate increases.

DISCUSSION

Both the experiments and the bulk flow model for this leakage path geometry indicate very little variation of the rotordynamic forces for different values of inlet swirl. This is possibly due to the viscous effects of the rotor, which may negate the effect of the inlet swirl velocity at any point in the leakage path not near the impeller tip.

The direct damping for the experiments exhibits a small peak at a flow coefficient of about $\phi = 0.02$. It is not clear why this effect is observed, however, the whirl ratio, k/C, appears to uniformly increase with increasing flow coefficient. The region of forward subsynchronous whirl in which the average tangential force is destablizing does not appear to be affected by this peak in one of the tangential force coefficients.

CONCLUSIONS

The influence of discharge-to-suction leakage inlet swirl on the rotordynamic forces in a typical shrouded centrifugal pump has been investigated. It was observed that the ratio of inlet tangential velocity to the tip velocity did not significantly affect the behavior of the unsteady forces for a given leakage flow rate. The region of forward whirl ratios for which the tangential force is destabilizing was found to increase with increasing flow rate for a rotor shape which forms a typical leakage path geometry. Finally, the bulk flow model developed by Childs, with some modification, can be made to match the experimental data at low flow coefficients.

ACKNOWLEDGEMENTS

The authors wish to thank the Advanced Rotating Machinery group of Rocketdyne division of Rockwell Aerospace for financial support and assistance.

REFERENCES

Adkins, D. and Brennen, C., 1988, Analysis of Hydrodynamic Radial Forces on Centrifugal Pump Impellers, ASME *Journal of Fluids Engineering*, Vol. 110, No. 1, pp. 20-28.

Baskharone, E., and Hensel, S., 1993, Flow Field in the Secondary, Seal-Containing Passages of Centrifugal Pumps, ASME *Journal of Fluids Engineering*, Vol. 115, pp. 702-709.

Childs, D., 1989, Fluid-Structure Interation Forces at Pump-Impeller-Shroud Surfaces for Rotordynamic Calculations, ASME *Journal of Vibrations, Acoustics, Stress, and Reliablity in Design*, Vol. 111, pp. 216-225.

Guinzburg, A., 1992, Rotordynamic Forces Generated By Discharge-to-Suction Leakage Flows in Centrifugal Pumps, Ph.D. Thesis, California Institute of Technology.

Guinzburg, A., Brennen, C,, Acosta, A., and Caughey, T., 1993, The Effect of Inlet Swirl on the Rotordynamic Shroud Forces in a Centrifugal Pump, ASME *Journal of Engineering for Gas Turbines and Power*, Vol. 115, No. 2, pp. 287-293.

Guinzburg, A., Brennen, C,, Acosta, A., and Caughey, T., 1994, Experimental Results for the Rotordynamic Characteristics of Leakage Flows in Centrifugal Pumps, ASME *Journal of Fluids Engineering*, Vol. 116, No. 1, pp. 110-115.

Hirs, G., 1973, A Bulk-Flow Theory For Turbulence in Lubricant Films, ASME *Journal of Lubrication Technology*, April, pp.137-146.

Jery, B., 1986, Experimental Study of Unsteady Hydrodynamic Force Matrices on Whirling Centrifugal Pump Impellers, Ph.D. Thesis, California Institute of Technology.

Sivo, J., Acosta, A., Brennen, C., Caughey, T., Ferguson, T., and Lee, G., 1994, Laser Velocimeter Measurements in the Leakage Annulus of a Whirling Centrifugal Pump, ASME *Laser Anemometry-1994, Advances and Applications* FED-Vol. 191, pp. 111-117.

Sivo, J., Acosta, A., Brennen, C., and Caughey, T., 1995, The Influence of Swirl Brakes on the Rotordynamic Forces Generated by Discharge-to-Suction Leakage Flows in Centrifugal Pumps, ASME *Journal of Fluids Engineering*, Vol. 117, No. 1, pp. 104-108.

Yamada, Y., 1962, Resistance of Flow Through an Annulus with an Inner Rotating Cylinder, *Bulletin of JSME*, Vol. 5, pp. 302-310.

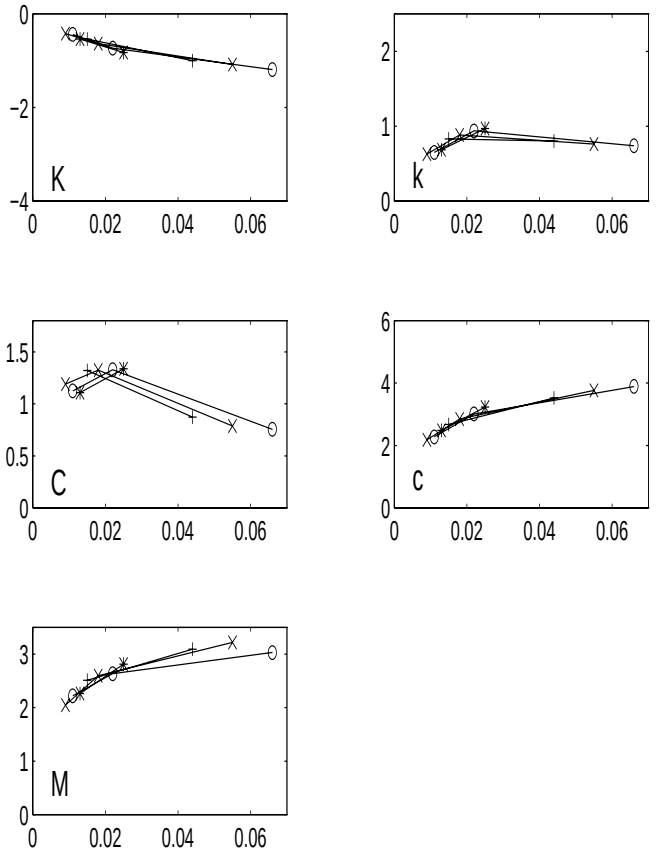

FIGURE 4: Rotordynamic force coefficients plotted against flow coefficient ϕ for the experimental tests with , = 0.4(+), 0.5(x), 0.6(o), and 0.7(*). Experimental error for all coefficients is 5% except for K which is 8%.

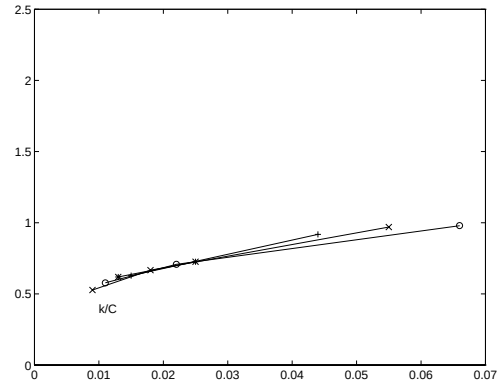

FIGURE 5: Whirl ratio plotted against ϕ for the experimental tests with , = 0.4(+), 0.5(x), 0.6(o), and 0.7(*).

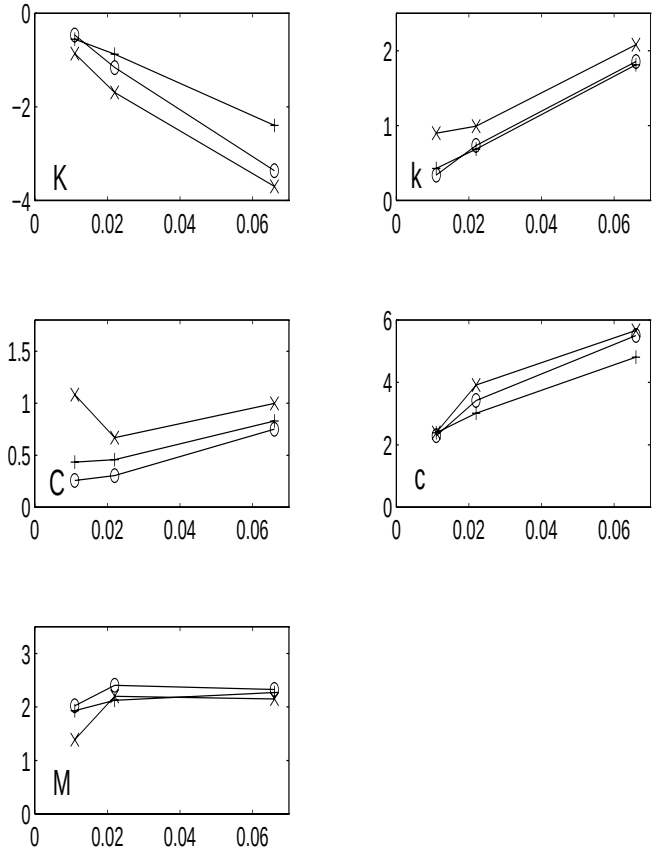

FIGURE 6: Rotordynamic force coefficients plotted against ϕ for Childs' model with $ns = 0.13$, $nr = 0.08$ (+), $ns = 0.08$, $nr = 0.13$ (x), and $ns = 0.08$, $nr = 0.01$ (o).

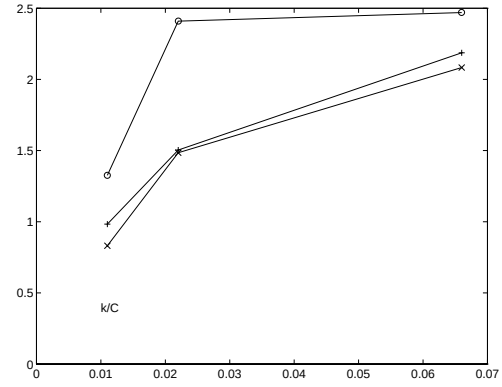

FIGURE 7: Whirl ratio plotted against ϕ for Childs' model with $ns = 0.13$, $nr = 0.08$ (+), $ns = 0.08$, $nr = 0.13$ (x), and $ns = 0.08$, $nr = 0.01$ (o).